ACS APPLIED MATERIALS & INTERFACES

Research Article

www.acsami.org

Synthesis, Characterization, and Fluorescence Properties of Mixed Molecular Multilayer Films of BODIPY and Zn(II) Tetraphenylporphyrins

Michael R. Topka and Peter H. Dinolfo*

Department of Chemistry and Chemical Biology, Rensselaer Polytechnic Institute, 110 Eighth Street, Troy, New York 12180, United States

Supporting Information

ABSTRACT: A new azido functionalized 4,4-difluoro-4-bora-3*a*,4*a*-diaza-*s*-indacene (**BODIPY**) has been synthesized to achieve spectral complementarity to a Zn(II) tetraphenylethynyl porphyrin (**ZnTPEP**). Mixed multilayer films were assembled on glass and quartz up to 10 bilayers thick in a layer-by-layer (LbL) fabrication process using copper(I)-catalyzed azide-alkyne cycloaddition (**CuAAC**) to couple these two dyes together with a tris-azido linker. By varying the amount of **BODIPY** in the **CuAAC** reaction solutions for the azido linker layers, we achieve tunable doping of **BODIPY** within the porphyrin films. We are able to demonstrate linear film growth and determine thickness by X-ray reflectivity (XRR). XRR data indicated that lower **BODIPY** loading leads to higher porphyrin content and slightly thicker films. Fluorescence emission and excitation spectra of the mixed multilayer films show efficient quenching of the **BODIPY** singlet and enhanced **ZnTPEP** emission, suggesting efficient energy transfer (EnT). The ease of fabrication and tunability of these films may serve as potential light harvesting arrays for molecular-based solar cells.

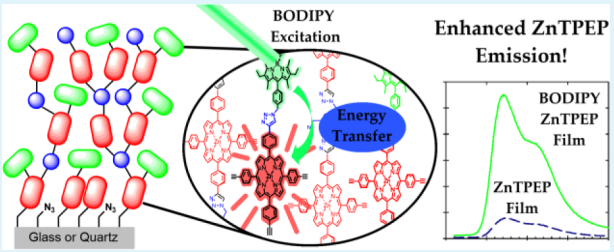

KEYWORDS: *porphyrin, bodipy, light harvesting, layer-by-layer, multilayer films, thin films, energy transfer*

INTRODUCTION

Light harvesting arrays (LHAs) are central elements of artificial photosynthetic devices and photoelectrochemical cells that are assembled using molecular components.[1−4] A common approach to designing such systems is to model them after the biomolecules responsible for natural photosynthesis, where various antenna pigments are employed to absorb sunlight and transfer that energy to a reaction center with near perfect efficiency. Fabrication of these donor−acceptor arrays often requires lengthy synthetic procedures before incorporation of the precoupled dyes into artificial photosynthetic devices and solar cells.[5,6] In an effort to facilitate the incorporation of donor−acceptor systems into devices for solar energy conversion, we have developed a layer-by-layer (LbL) technique to modify electrode and semiconductor surfaces with discrete molecular layers. The coupling methodology utilized to attach these chromophores together is copper(I)-catalyzed azide−alkyne cycloaddition (**CuAAC**).[7] In this process, the dyes are linked together with a stable, regioselective 1,4-triazole heterocycle. We have utilized this click-chemistry-based LbL methodology to modify numerous surfaces with porphyrin-based and perylene-diimide-based multilayered thin films.[8−13] The development of these light harvesting arrays requires a fundamental understanding of the structural−functional relationship between various donor and acceptor chromophores at interfaces for solar applications.

We want to explore the energy transfer (EnT) between adjacent chromophores in thin films toward application in broadband photoelectrochemical cells. This efficient coupling method allows us to control the molecular architecture to modified surfaces on a nanometer scale. These components would direct or transfer that energy toward the semiconductor electrode surface for use in electrochemical processes.

We are currently interested in studying molecular-based EnT systems employing porphyrin building blocks due to their resemblance to chlorophylls found in natural systems.[14−16] Porphyrins are an attractive chromophore due to their strong absorbance in the blue and red regions of the visible spectrum (the Soret and Q-bands, respectively).[17,18] However, they lack any significant absorption in the green region of the visible spectrum (450−550 nm). To obtain panchromatic absorption, an attractive route is to use donor−acceptor arrays that harvest or absorb a large fraction of the solar spectrum.[19−21]

A popular green absorbing donor chromophore used in these arrays is the 4,4-difluoro-4-bora-3*a*,4*a*-diaza-*s*-indacene, or **BODIPY**.[22,23] **BODIPY** is an accessory pigment that can act as an antenna light harvesting chromophore to absorb light in the green spectrum, where the porphyrin lacks significant

Received: January 18, 2015
Accepted: March 26, 2015
Published: March 26, 2015

DOI: 10.1021/acsami.5b00519
ACS Appl. Mater. Interfaces 2015, 7, 8053−8060

Scheme 1

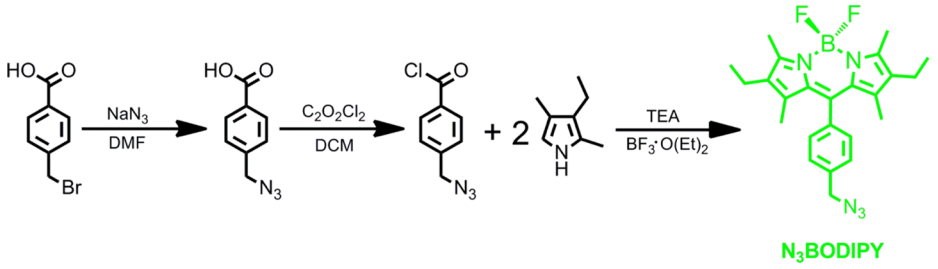

Scheme 2

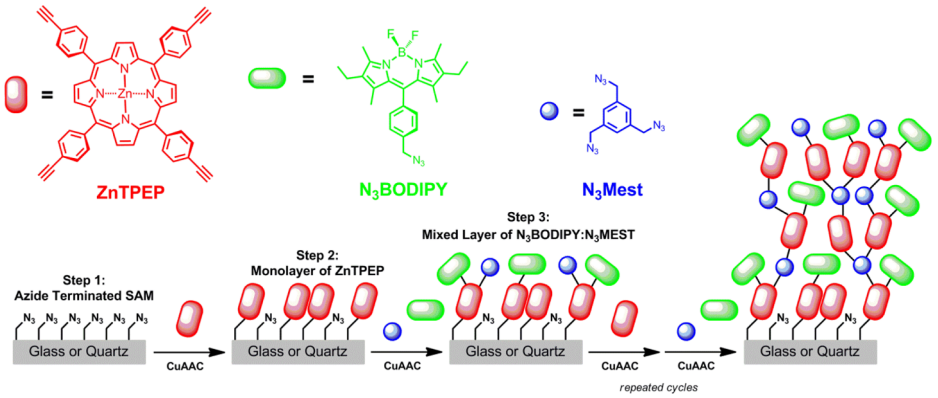

absorption. This chromophore exhibits a strong absorbance feature in the 400−600 nm range, relatively long-lived singlet excited states, and high singlet fluorescence quantum yields.[23] Additionally, the singlet $\pi-\pi^*$ transition is tunable via the modification of the pyrrole groups of the **BODIPY** core.[22] Numerous examples of donor−acceptor arrays have been reported using the **BODIPY**−porphyrin combination, including various covalent connections such as cyanuric chloride bridges[24] and phenyl−ethynyl bridges,[25,26] as well as electrostatic interactions[27,28] and metal−organic frameworks.[29] We have recently described one such system utilizing 1,4-triazole linkages formed from **CuAAC** reactions that showed >95% EnT efficiency.[30] Others have also employed **CuAAC** reactions to link porphyrin and **BODIPY** chromophores together.[31−33] Herein, we report the synthesis and characterization of mixed multilayer films of an azido-modified **BODIPY** (**N_3BODIPY**) and Zn(II) 5,10,15,20-tetra(4-ethynylphenyl)porphyrin (**ZnTPEP**) at different donor−acceptor ratios grown using a slightly modified LbL method. We utilized the tunability of **BODIPY** chromophores with the addition of an ethyl group on the 3,3′ positions to red-shift the singlet absorbance and fluorescence emission spectra. This provides enhanced spectral overlap of the **N_3BODIPY** fluorescence emission with the Q-band absorbance of **ZnTPEP**. This should allow for more efficient Förster resonance energy transfer (FRET) through the donor−acceptor array. Additionally, these chromophores have excellent spectral complementarity and thus allow for selective excitation of the donor chromophore independent of the acceptor chromophore. The multilayer arrays display linear growth with three different loadings of **N_3BODIPY** within the film as determined by absorbance spectroscopy and X-ray reflectivity (XRR) measurements. We found that the antenna **N_3BODIPY** chromophore effectively increased the green-light absorptivity of the films. Fluorescence emission and excitation spectra of the mixed multilayer films show efficient quenching of the **BODIPY** singlet emission and enhanced **ZnTPEP** emission, suggesting efficient EnT.

RESULTS AND DISCUSSION

Dye Synthesis. **ZnTPEP** and **N_3Mest** [1,3,5-tris-(azidomethyl)benzene] were available from previous studies.[8] **N_3BODIPY** was synthesized similarly according to literature procedures (Scheme 1).[34] Briefly, 4-(bromomethyl)benzoic acid was converted to an azide by stirring with NaN_3 in DMF, followed by reaction with oxalyl chloride to generate the acyl chloride. Next, freshly distilled 2,4-dimethyl-3-ethyl-pyrrole was added and stirred at room temperature for 3 days. Finally, triethylamine and boron trifluoride diethyl etherate were added and stirred for an additional day. Purification on silica gel afforded the product in decent yields [overall yield from 4-(bromomethyl)benzoic acid was 15%].

Multilayer Growth. Mixed multilayers of **ZnTPEP**, **N_3BODIPY**, and **N_3Mest** were formed in a layer-by-layer (LbL) methodology on glass and quartz substrates using the **CuAAC** assembly technique described previously, but with a slight modification (Scheme 2).[8−13] Briefly, the LbL fabrication process starts by functionalizing either glass or quartz with an azido-terminated alkyl siloxane self-assembled monolayer. The LbL technique utilizes two sequential self-limiting surface **CuAAC** reactions to control layer growth on the molecular scale. **ZnTPEP** reacts with the azide-rich functionalized surface, replacing the surface with ethynyls (step 2). Next, a mixed solution containing a specific ratio of a multi-azido linker (**N_3Mest**) and mono-azido dye (**N_3BODIPY**) is introduced to the surface for another **CuAAC** reaction to take place (step 3). Some **N_3Mest** clicks onto the surface, which allows for the generation of another reaction with **ZnTPEP** as azide functionality is replenished again. This mixed multilayer process uses the dendritic nature of both **ZnTPEP** and **N_3Mest** to ensure continued linear multilayer growth. Upon mixing

DOI: 10.1021/acsami.5b00519
ACS Appl. Mater. Interfaces 2015, 7, 8053−8060

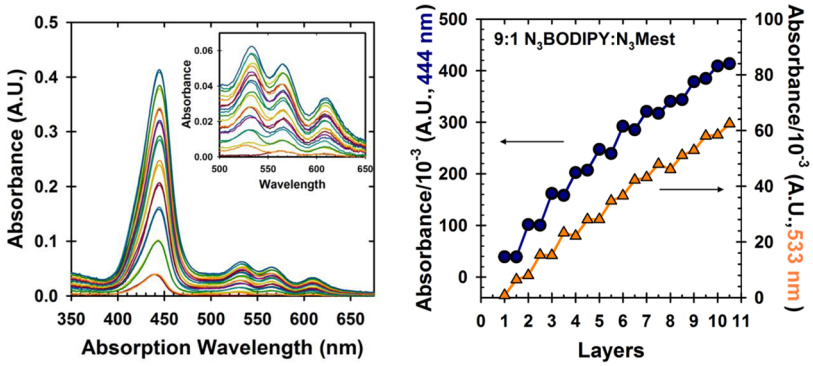

Figure 1. Left: UV−vis absorbance profiles of each layer for 10 bilayers of **ZnTPEP**, **N_3BODIPY**, and **N_3Mest** on glass. Inset shows a zoomed plot from 500 to 650 nm. Right: Absorbance at 444 nm (dark blue circles) and 533 nm (orange triangles) vs layers.

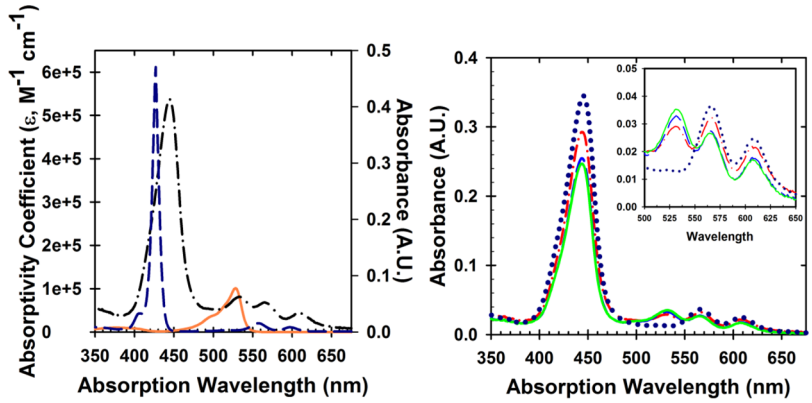

Figure 2. Left: Solution UV−vis absorbance spectrum of **N_3BODIPY** (solid orange line) and **ZnTPEP** (dashed dark blue line) in dry THF overlaid with 10 bilayer profile of a slide containing **ZnTPEP** and the 9:1 ratio of **N_3BODIPY** to **N_3Mest** (dash−dotted black line) on a glass surface. Right: The absorbance spectra of 6 bilayers of **ZnTPEP** and 9:1 (green solid line), 6:1 (blue dashed line), and 3:1 (red dash−dotted line) **N_3BODIPY:N_3Mest**, along with **ZnTPEP** (dark blue dotted line) on quartz. Inset shows a zoomed region from 500 to 650 nm highlighting the results of the different doping levels of **N_3BODIPY** in the multilayer films.

N_3BODIPY into the linker reactions, we assume that reaction with **ZnTPEP** may cap chain growth, but the tris-azido functionality of **N_3Mest** will enable addition of subsequent **ZnTPEP** layers by replenishing the surface azide content. Increasing the ratio of **N_3BODIPY** to **N_3Mest** will lead to higher **BODIPY** loading but ultimately limit the subsequent **ZnTPEP** coverage. Repeating steps 2 and 3 generates bilayers of donor−acceptor dyes to a desired thickness or optical density. From here on, we will refer to a single bilayer consisting of one layer of **ZnTPEP** acceptor (whole integers) and one mixed azido layer containing the **N_3BODIPY** donor and the **N_3Mest** linker (half integers).

Figure 1 shows the absorbance profiles of each layer in a 10 bilayer mixed multilayer film with a 9:1 molar ratio of **N_3BODIPY** to **N_3Mest** on glass. The inset and right plot of Figure 1 show the alternating behavior of porphyrin growth followed by **BODIPY** growth. Varying the ratio of **N_3BODIPY** to **N_3Mest** allows for a controlled doping level of donor into the arrays. By varying the ratio of **N_3BODIPY** to **N_3Mest**, we are able to control the amount of **BODIPY** incorporated into the films. In addition to the 9:1 ratio, we used 3:1 and 6:1 ratios, and were able to achieve up to 10 linear bilayers (Supporting Information Figure S1). The combination of **N_3Mest** containing 3 times the azide content per molecule compared to **N_3BODIPY** and the slightly lower reactivity of **N_3BODIPY** required each mixed layer reaction to have a higher concentration of **N_3BODIPY** than **N_3Mest** in order to successfully dope **BODIPY** into the multilayer films.

Electronic Absorption Analysis. Figure 1 demonstrates the LbL multilayer growth between the donor and acceptor chromophores. The strong absorbance at 444 nm is the Soret band from **ZnTPEP**, while the smaller peak at 533 nm is from **N_3BODIPY**. The second plot shows the alternating growth between these two chromophores upon LbL assembly. Furthermore, the last two smaller peaks are the Q-band features from the **ZnTPEP**. The inset of Figure 2 shows the alternating growth between the first Q-band of the **ZnTPEP** and the growth of the **N_3BODIPY** into the mixed donor−acceptor film. Supporting Information Figure S2 (left) tracks the growth rate among the Soret band, **BODIPY** peak, and the Q-bands of the two chromophores together. Because of the higher absorptivity of the Soret band, we see that the absorbance growth rate is much higher than that of the other two absorbance features of the film. Additionally, the **BODIPY** feature in Supporting Information Figure S2 (right) has a growth rate higher than those of the subsequent lower energy Q-bands which corresponds to the solution absorptivity coefficients (Figure 2).

The left graph in Figure 2 compares 10 bilayers of **ZnTPEP** and a 9:1 ratio of **N_3BODIPY** to **N_3Mest** on glass with that of the corresponding molecular components in THF. The film reflects the combined spectral features of both chromophores; however, the absorbance profile of the film shows a significant

DOI: 10.1021/acsami.5b00519
ACS Appl. Mater. Interfaces 2015, 7, 8053−8060

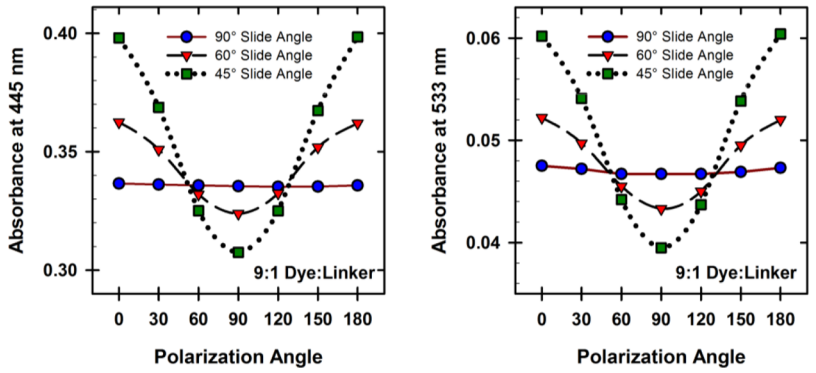

Figure 3. Peak absorbance of **ZnTPEP** and 9:1 **N_3BODIPY**:**N_3Mest** on glass at 445 nm (left) and 533 nm (right) as a function of polarization angle of the incident light and the angle of the slide with respect to the incident light path.

bathochromic shift and broadening compared to the solution spectrum. These changes in the Soret and Q-bands of the porphyrin are typical of J-type aggregates. This has been predicted by exciton theory[35] and has been previously reported for multilayers of **ZnTPEP**.[8,10] As a result, the porphyrin has the same ability to pack closely on the surface in the mixed layers, compared to the homogeneous porphyrin films, even with the inclusion of the **BODIPY** chromophores with the linker layers. The slight red-shift at the **BODIPY** absorbance has been reported on other films of **BODIPY** chromophores.[36]

As the doping level of **BODIPY** within the films is increased, the amount of porphyrin decreases as observed from the optical absorption spectra (right graph in Figure 2 and Supporting Information Figure S1). This phenomenon can be explained by the different ratio of **BODIPY** to **N_3Mest**. Consequently, as we increase the amount of **BODIPY** within the films, the amount of **N_3Mest** decreases. This has a direct effect on the amount of porphyrin that is able to react in the subsequent layer. With decreased azide content on the surface, fewer porphyrins are able to react on the substrate, which is reflected by the lower overall absorbance per layer for more highly **BODIPY**-doped films. Supporting Information Figure S3 shows the decreased porphyrin growth as the **BODIPY** content increases.

A comparison of the absorbance values of **ZnTPEP** to **N_3BODIPY** in the multilayer films can be used to provide a rough estimate of the molar ratio of the two chromophores on the surface using their molar absorptivity coefficients.[37] Difference absorbance spectra of the mixed **ZnTPEP**–**N_3BODIPY** multilayer films from **ZnTPEP** films alone reveal the absorbance profile of **N_3BODIPY** in the films is nearly the same shape and width as that of **N_3BODIPY** in solution (Supporting Information Figure S4). Therefore, the solution molar absorptivity can be used as a reasonable estimate of surface coverage. The aggregation induced broadening of the absorbance profile of **ZnTPEP** films, on the other hand, will lead to a change in the molar absorptivity on the surface. We used a comparison of previously published electrochemically derived surface coverage data and absorbance spectra for multilayers of just **ZnTPEP** to calculate a surface molar absorptivity.[10] Using these values and comparing the absorbance spectra (right graph in Figure 2), we estimate an **N_3BODIPY**–**ZnTPEP** molar ratio of 0.26, 0.30, and 0.31 for mixed multilayer films grown using the 3:1, 6:1, and 9:1 **N_3BODIPY**–**N_3Mest** mixture in the linker reaction steps, respectively.

Polarized UV–vis was also employed to study structure in the donor–acceptor films. Figure 3 outlines a typical polarized experiment for the 9:1 ratio film. Polarized light was changed in 30° increments while the slide was held at 45°, 60°, and 90° angles to the incident light. At non-normal angles the slides show polarization dependence, while vertically polarized light (90°) shows decreased absorbance compared to horizontally polarized light (0°, 180°). In contrast, when the slide was held at normal, there was no change in absorbance. This same effect was seen for the other two slides (Supporting Information Figure S5). The polarization anisotropy at incidence angles non-normal to the slide and the lack thereof at normal incidence are consistent with a preferential orientation of the electronic transition dipoles (and therefore the porphyrin plane) with respect to the surface normal, but no orientation preference in the plane of the substrate surface. An average angle between the electronic absorbance dipole and the substrate can be determined using the polarization absorbance values as described elsewhere.[10,12] Using the dichroic ratio between the horizontally and vertically polarized light absorbance, we estimate the angle of the porphyrin absorption transition dipole moment to be 40.2°, 40.6°, and 40.8° to the surface when the slide was held at a 45° to the incident light. This result is very similar to previously reported angles of **ZnTPEP** on glass from polarization absorbance and polarized FTIR on ITO.[10] Similarly calculated were the absorption transition dipole moment angles for the **N_3BODIPY** which were 29.4°, 33.0°, and 31.2°. The evidence of polarization dependence indicates that there is some order in the multilayer films and that introducing **N_3BODIPY** between the porphyrin layers does not significantly disrupt the structure of these films.

X-ray Reflectivity Analysis. XRR was employed to probe the thickness, roughness, and density of the multilayer films on quartz. This technique has been used to probe multilayer films composed of other molecular building blocks,[38−41] in addition to **ZnTPEP** multilayers assembled via the **CuAAC** method.[8,9] Briefly, the specular reflectance of X-rays off various interfaces of the thin film and substrate results in interference patterns as the angle of incident changes. The dependence of the position of the interference patterns or Kiessig fringes on thickness and electron density of the thin film can be modeled using the Bragg equation.[42,43] The XRR curves were analyzed and simulated using the LEPTOS software suite from Bruker AXS. A sample model was constructed to generate the simulated curve (red solid line) which was compared to the data (black dots) as seen in Figure 4. The model was composed of the following simulated layers: (1) bulk SiO_2, (2) carbon material layer representing the alkane self-assembled monolayer, and (3) the mixed organic dye layer constructed by **CuAAC**. Table 1

DOI: 10.1021/acsami.5b00519
ACS Appl. Mater. Interfaces 2015, 7, 8053−8060

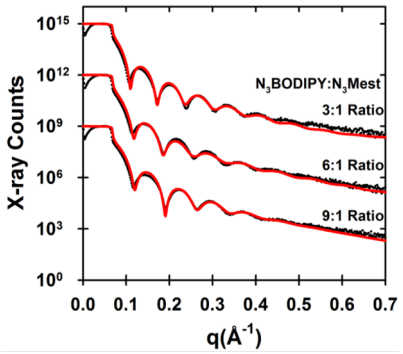

Figure 4. XRR curves (black dots) and the simulated fits (red solid line) for the three mixed multilayer films on glass containing **ZnTPEP** and 9:1, 6:1, and 3:1 reaction ratios of **N_3BODIPY:N_3Mest**. The XRR data for the films with a 6:1 and 3:1 ratio are offset for clarity.

Table 1. Thickness, Surface Roughness, and Mass Density Parameters Derived from Simulating and Fitting XRR Data from Figure 4

film	thickness (nm)	roughness (nm)	density (g/cm^3)	abs at Soret max (au)	thickness per bilayer (nm)
ZnTPEP[44]	17.4	1.00	1.00	N/A	1.7
3:1 ratio	16.8	0.50	1.18	0.48	1.6
6:1 ratio	15.3	0.39	0.96	0.43	1.5
9:1 ratio	15.0	0.36	1.11	0.41	1.5

shows the resulting thickness, roughness, and density values of the multilayer films derived from the simulated XRR curves. The overall amount of porphyrin appears to be the controlling factor for the thickness of the multichromophoric films. As seen in Table 1, this thickness is typical of multilayer films of **ZnTPEP**[9] on Si(100). The higher roughness for the **ZnTPEP** film can be attributed to the increased porphyrin content. Roughly, the densities for all three layers are consistent throughout each 10 bilayer sample within fitting and experimental error.

Fluorescence Spectroscopy Analysis. Fluorescence excitation and emission spectra for each film were collected to explore EnT properties of the donor–acceptor multilayers. To decrease background scattering, 6 bilayers of each film were grown on quartz (right graph in Figure 2) and showed similar absorbance growth profiles as in Figure 1 and Supporting Information Figure S1. Figure 5 shows the typical emission spectra resulting from excitation of the Soret band (dotted dark blue line) and from the higher energy Q-band of **ZnTPEP** (solid orange line) for the 9:1 ratio thin film. Promotion of both the S2 and S1 states of the **ZnTPEP** shows no spectral shift for the emission peak at 624 nm and the shoulder at 664 nm. Similar to those of the absorbance spectra, the emission peaks for the porphyrin are also bathochromically shifted, as seen in Figure 5 (dashed orange line) as compared to solution measurement (black solid line). Similar results were also seen for the other two ratio films.

Upon excitation of the mixed multilayer films at 530 nm, where only **N_3BODIPY** absorbs significantly, we observe emission exclusively from the porphyrin at 624 and 664 nm (Figure 6). No emission from the **N_3BODIPY** is seen in the range 550–590 nm. The lack of detectable emission from **N_3BODIPY** could be the result of aggregation induced quenching[45,46] due to the lack of large bulky substituents in

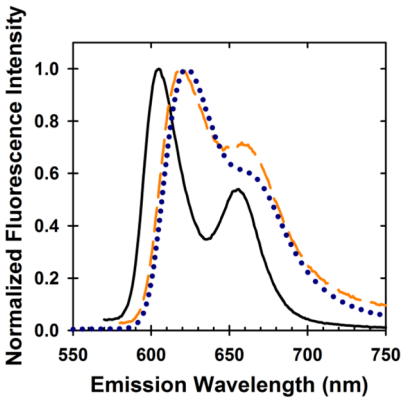

Figure 5. Emission spectra of six bilayers of **ZnTPEP** and 9:1 **N_3BODIPY:N_3Mest** on quartz excited at 444 nm (dotted dark blue line) and 558 nm (Q_{1-0}, dashed orange line) normalized by emission maxima. The solid black line is **ZnTPEP** in dry THF excited at 556 nm, which is also normalized by emission maximum.

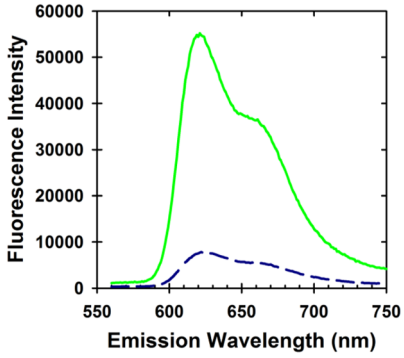

Figure 6. Emission spectra of six mixed bilayers of **ZnTPEP** and 9:1 **N_3BODIPY:N_3Mest** on quartz excited at the **N_3BODIPY** absorance peak at 530 nm (green solid line). The dark blue dashed line shows the emission profile of six bilayers of only **ZnTPEP** on quartz excited at 530 nm in comparison.

the 3,3′ positions.[36,47] Alternatively, **N_3BODIPY** emission quenching could be due to nearly quantitative EnT to the porphyrin acceptor via FRET- or Dexter-type mechanisms. Our previous studies on **BODIPY–ZnTPP** donor–acceptor systems in solution predicted a Förster radius of about 3 nm on the basis of spectral overlap.[30] This distance is approximately double that of a bilayer thickness (1.5–1.6 nm, Table 1). This arrangement would put the donor–acceptor chromophores in close contact, potentially leading to high EnT efficiencies. Using the mass density obtained from XRR data fitting (Table 1) and the approximate molar ratio of **N_3BODIPY–ZnTPEP** for each of the three films, we estimate the number of porphyrin acceptor **ZnTPEP** molecules within a given 3 nm radius sphere to range from 57 to 71. The complete quenching of the **N_3BODIPY** donor emission is consistent with a FRET mechanism given the large number of **ZnTPEP** acceptors within the Förster radius.

For further elucidation of the contribution of **ZnTPEP** fluorescence coming from the **N_3BODIPY**, excitation spectra were taken for the three films. If EnT does occur, there should be significant contribution from not only the **ZnTPEP** absorption features but also those of the **N_3BODIPY**. Porphyrin emission was monitored at 624 nm, and the resulting spectra were obtained in Figure 7. The Soret band

DOI: 10.1021/acsami.5b00519
ACS Appl. Mater. Interfaces 2015, 7, 8053–8060

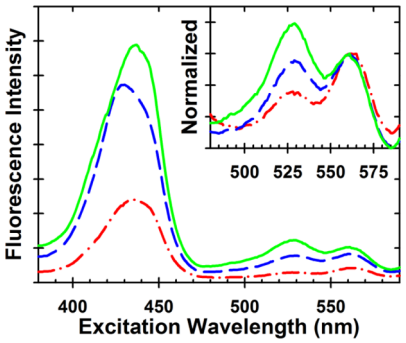

Figure 7. Excitation spectra of **ZnTPEP** and 9:1 (green solid line), 6:1 (blue dashed line), and 3:1 (red dash−dotted line) **N_3BODIPY**:**N_3Mest** on quartz monitored at porphyrin emission at 624 nm. Inset shows a zoomed region excitation profiles normalized at the first Q-band highlighting the results of the different doping levels of **N_3BODIPY** in the thin films.

absorption is very pronounced and easily seen at around 430 nm while the first Q-band at around 565 nm corresponds very well to the absorption maximum obtained in Figure 1. Differences in the overall intensities between the three films are most likely due to varying amounts of aggregation within the film. In addition, a peak around 530 nm represents the **N_3BODIPY** absorption peak. Figure 7 (inset) shows the excitation spectra normalized to the Q_{1-0} band, which reflects the different loading of the **N_3BODIPY** dyes onto the surface. The presence of this peak indicates that the **N_3BODIPY** dyes embedded within the films are contributing to the overall film fluorescence. Taken together, the fluorescence excitation and emission data provide strong evidence for efficient EnT properties of these mixed multilayer films.

CONCLUSION

Successful incorporation of a new azido functionalized **BODIPY** into dense multilayers of **ZnTPEP** has been performed using the LbL **CuAAC**-based methodology. Changing the ratio of a tris-azido linker to **BODIPY** in the click solution can change the doping level of the **BODIPY** incorporated into the film. We are able to demonstrate very controlled growth of these mixed multilayers up to 10 bilayers and have shown that these films resembled previous films of **ZnTPEP**. These films were characterized by UV−vis absorption, polarized electronic absorption, X-ray reflectivity, and fluorescence emission and excitation. Polarization studies showed a strong dependence on the orientation of the film to the light path, which indicated preferential orientation of **ZnTPEP** on a surface with typical angles of about 40°. X-ray reflectivity also revealed that these films have thicknesses similar to those of other porphyrin films. Fluorescence studies show the EnT properties that these films have and show the potential to utilize the **CuAAC** layer-by-layer method to generate multichromophoric energy transfer assemblies designed to develop full spectral light harvesting materials toward the development of more efficient DSSCs.

EXPERIMENTAL SECTION

General Methods. NMR spectra were obtained on a Varian 500 MHz spectrometer, and chemical shifts were referenced to that of the solvent. HR ESI MS spectra were obtained on a Thermo Electron Finnigan TSQ Quantum Ultra.

Materials. Solvents, ACS grade or better, were purchased form Sigma-Aldrich or Fisher Scientific and used as received unless specified. Toluene was purged with nitrogen and dried over 4 Å molecular sieves before use. Sodium ascorbate (Aldrich) and other chemicals were also used as received. 11-Azidoundecyltrimethoxysilane, 1,3,5-tris(azidomethyl)-benzene (**N_3Mest**), **ZnTPEP**, tris(benzyltriazolylmethyl)amine (**TBTA**), 1,3,5-tris(hydroxypropyltriazolyl)amine (**THPTA**), and 4-(azidomethyl)-benzoic acid were available from previous studies or were synthesized according to literature methods.[8,48−51] Glass and quartz slides were purchased from SPI Supplies.

2,6-Diethyl-4,4-difluoro-8-(4-azidomethylphenyl)-1,3,5,7-tetramethyl-4-bora-3*a*,4*a*-diaza-*s*-indacence (N_3BODIPY). The product was made according to similar literature methods.[34,52] 4-(Azidomethyl)benzoic acid (1.0 g, 5.6 mmol) was added to 120 mL of dry DCM under a nitrogen environment. Oxalyl chloride (0.8 mL, 9.3 mmol) and 5 drops of dry DMF were slowly added to the solution. The pale yellow reaction mixture was stirred under a nitrogen atmosphere for 24 h. The solvent and excess oxalyl chloride were removed by rotary evaporation with minimal contact to ambient atmosphere. To the residue was added 120 mL of dry DCM and freshly distilled 2,4-dimethyl-3-ethyl-1*H*-pyrrole (4.6 mL, 8.9 mmol) under a nitrogen atmosphere. The solution turned deep red within 5 min and was stirred for 5 days under nitrogen. Triethylamine (4.6 mL, 33.0 mmol) and boron trifluoride diethyl etherate (5.6 mL, 44.6 mmol) were added to the solution and allowed to stir for another day at room temperature. The solvent was removed under reduced pressure resulting in a dark red powder. Purification by chromatography (silica gel, 3:1 $CHCl_3$/hexanes) afforded the pure product as red crystals (294 mg, 15.1%). ^{1}H NMR ($CDCl_3$): δ 7.45 (d, 2H, J = 8.1 Hz), 7.34 (d, 2H, J = 8.1 Hz), 4.45 (s, 2H), 2.55 (s, 6H), 2.32 (q, 4H, J = 7.5 Hz), 1.29 (s, 6H), 0.99 (t, 6H, J = 7.5 Hz). HR-ESI MS m/z calculated for $[M + H]^+$ 436.2484; found $[M + H]^+$ 436.2480. UV−vis (THF) λ, nm (ε, M^{-1} cm^{-1}): 528 (101 100), 500 (sh, 38 000), 378 (b, 10 206).

Azido-SAM Formation on Glass and Quartz. Glass or quartz slides were washed sequentially with acetone, DCM, MeOH, and deionized (DI) water prior to exposure to a piranha solution for 30 min. Piranha solution consists of a 3:1 v/v concentrated sulfuric acid to 30% hydrogen peroxide. (***Caution!*** *Piranha is a strong oxidizer and will react violently with most organic materials. Proper handling and caution are required.*) The slides were rinsed with copious amounts of DI water, dried under a stream of nitrogen, and placed in a Schlenk flask at a pressure of ~10^{-3} Torr to remove residual surface water for at least 1 h. Nitrogen was replaced in the flask, and a solution of approximately 1 mM 11-azidoundecyltrimethoxysilane in anhydrous toluene was added to the flask and heated to 65−70 °C for 12 h. After the slides cooled to room temperature, they were sonicated in fresh toluene for 5 min; washed sequentially with toluene, acetone, DCM, MeOH, and DI water; and dried with a stream of nitrogen. Finally, the slides were placed in an oven at 75 °C under 10^{-3} Torr and dried for 3 h.

Multilayer Fabrication. *Layer Additions of **ZnTPEP**.* A solution of DMSO containing ~4.8% water, 1.29 mM **ZnTPEP**, 0.32 mM $CuSO_4$, 0.35 mM TBTA, and 0.48 mM sodium ascorbate was placed in contact with one side of a SAM functionalized slide. After 10 min, the slide was washed with acetone, DCM, 5 mM disodium ethylenediamine tetraacetate in 50/50 EtOH/DI water, 5 mM diethyldithiocarbamate in 50/50 MeOH/DI water, MeOH, and finally DI water.

*Layer Additions of **N_3BODIPY** and **N_3Mest**.* A solution of DMSO containing ~32% water; 2.60 mM **N_3BODIPY**; either 0.87, 0.43, or 0.29 mM **N_3Mest**; 5.20 mM $CuSO_4$; 5.71 mM TBTA; and 10.39 mM sodium ascorbate was placed in contact with one side of a SAM functionalized slide. After 10 min, the slide was washed with acetone, DCM, 5 mM disodium ethylenediamine tetraacetate in 50/50 EtOH/DI water, 5 mM diethyldithiocarbamate in 50/50 MeOH/DI water, MeOH, and finally DI water.

Electronic Absorption Spectroscopy. UV−vis electronic absorption spectra were taken on a Perkin-Elmer Lambda 950 UV−

DOI: 10.1021/acsami.5b00519
ACS Appl. Mater. Interfaces 2015, 7, 8053−8060

vis spectrometer with slides held normal to the incident light beam in air. Samples were background subtracted using a SAM functionalized glass or quartz slide. Polarized absorbance spectra were taken with the thin film sample along with a corresponding SAM background positioned at 45°, 60°, and 90° angles with respect to the incident light. The incident light was polarized using a Glen-Taylor prism.

Specular X-ray Reflectivity. Specular X-ray reflectivity (XRR) experiments were performed on a Bruker D8 Discover X-ray diffractometer using a 2-circle $\theta/2\theta$ goniometer, a centric Eulerian cradle, and a sealed copper tube X-ray source (Cu Kα, λ = 1.54 Å) operated at 40 kV. The XRR curves were simulated using the Bruker Leptos software suite with a model consisting of two sample layers on top of a SiO_2 substrate. The first layer represents the alkylsiloxane self-assembled monolayer which was fixed at 1.7 nm (experimentally determined by XRR) with a density of 0.85 g/cm^3. The other layer represented the mixed porphyrin/**BODIPY** bilayer film. Variables for thickness, roughness, and density were constrained to reasonable values, and the range for the fitting was restricted to the region just below the critical angle to a region where the fringe patterns could no longer be differentiated from the noise during the fitting process to generate fitted estimates.

Fluorescence Spectroscopy. Fluorescence spectra were taken on a Horiba-Scientific FluoroLog3-21 equipped with dual grating monochromator on the excitation side and a single monochromator for the emission side. The excitation and emission slit widths were set at 10/5 nm for the film samples. A 450 W xenon lamp was used as the light source. Emission was collected by a cooled R928P PMT detector with a photomultiplier voltage of 950 V. Slides were held normal to the incident light beam in air on a solid state sample holder, and emission was detected in the front-face geometry. Samples were background subtracted using SAM functionalized quartz. All spectra were obtained within the same day to minimize variations in excitation light intensity.

■ ASSOCIATED CONTENT

Supporting Information

Additional absorbance and polarized absorbance profiles, and excitation fluorescence spectra of the multilayers. This material is available free of charge via the Internet at http://pubs.acs.org.

■ AUTHOR INFORMATION

Corresponding Author

*E-mail: dinolp@rpi.edu.

Notes

The authors declare no competing financial interest.

■ ACKNOWLEDGMENTS

M.R.T. acknowledges a Wiseman Family Fellowship from Rensselaer Polytechnic Institute. This material is based upon work supported by the National Science Foundation under CHE-1255100.

■ REFERENCES

(1) Meyer, T. J. Chemical Approaches to Artificial Photosynthesis. *Acc. Chem. Res.* **1989**, *22*, 163−170.

(2) Alstrum-Acevedo, J. H.; Brennaman, M. K.; Meyer, T. J. Chemical Approaches to Artificial Photosynthesis. 2. *Inorg. Chem.* **2005**, *44*, 6802−6827.

(3) Huynh, M. H. V.; Dattelbaum, D. M.; Meyer, T. J. Exited State Electron and Energy Transfer in Molecular Assemblies. *Coord. Chem. Rev.* **2005**, *249*, 457−483.

(4) Wasielewski, M. R. Energy, Charge, and Spin Transport in Molecules and Self-Assembled Nanostructures Inspired by Photosynthesis. *J. Org. Chem.* **2006**, *71*, 5051−5066.

(5) Lee, C. Y.; Hupp, J. T. Dye Sensitized Solar Cells: TiO_2 Sensitization with a Bodipy-Porphyrin Antenna System. *Langmuir* **2009**, *26*, 3760−3765.

(6) Ooyama, Y.; Hagiwara, Y.; Mizumo, T.; Harima, Y.; Ohshita, J. Synthesis of Diphenylamino-Carbazole Substituted BODIPY Dyes and Their Photovoltaic Performance in Dye-Sensitized Solar Cells. *RSC Adv.* **2013**, *3*, 18099.

(7) Meldal, M.; Tornøe, C. W. Cu-Catalyzed Azide-Alkyne Cycloaddition. *Chem. Rev.* **2008**, *108*, 2952−3015.

(8) Palomaki, P. K. B.; Dinolfo, P. H. A Versatile Molecular Layer-by-Layer Thin Film Fabrication Technique Utilizing Copper(I)-Catalyzed Azide-Alkyne Cycloaddition. *Langmuir* **2010**, *26*, 9677−9685.

(9) Palomaki, P. K. B.; Krawicz, A.; Dinolfo, P. H. Thickness, Surface Morphology, and Optical Properties of Porphyrin Multilayer Thin Films Assembled on Si(100) Using Copper(I)-Catalyzed Azide-Alkyne Cycloaddition. *Langmuir* **2011**, *27*, 4613−4622.

(10) Palomaki, P. K. B.; Dinolfo, P. H. Structural Analysis of Porphyrin Multilayer Films on ITO Assembled Using Copper(I)-Catalyzed Azide-Alkyne Cycloaddition by ATR IR. *ACS Appl. Mater. Interfaces* **2011**, *3*, 4703−4713.

(11) Palomaki, P. K. B.; Civic, M. R.; Dinolfo, P. H. Photocurrent Enhancement by Multilayered Porphyrin Sensitizers in a Photoelectrochemical Cell. *ACS Appl. Mater. Interfaces* **2013**, *5*, 7604−7612.

(12) Beauvilliers, E. E.; Topka, M. R.; Dinolfo, P. H. Synthesis and Characterization of Perylene Diimide Based Molecular Multilayers Using CuAAC: Towards Panchromatic Assemblies. *RSC Adv.* **2014**, *4*, 32866.

(13) Krawicz, A.; Palazzo, J.; Wang, G.-C.; Dinolfo, P. H. Layer-by-Layer Assembly of Zn(ii) and Ni(ii) 5,10,15,20-tetra(4-Ethynylphenyl)porphyrin Multilayers on Au Using Copper Catalyzed Azide-Alkyne Cycloaddition. *RSC Adv.* **2012**, *2*, 7513−7522.

(14) Schwarz, F. P.; Gouterman, M.; Muljiani, Z.; H. Dolphin, D. Energy Transfer between Covalently Linked Metal Porphyrins. *Bioinorg. Chem.* **1972**, *2*, 1−32.

(15) Li, J.; Lindsey, J. S. Efficient Synthesis of Light-Harvesting Arrays Composed of Eight Porphyrins and One Phthalocyanine. *J. Org. Chem.* **1999**, *64*, 9101−9108.

(16) S. Lindsey, J.; Prathapan, S.; E. Johnson, T.; W. Wagner, R. Porphyrin Building Blocks for Modular Construction of Bioorganic Model Systems. *Tetrahedron* **1994**, *50*, 8941−8968.

(17) Gouterman, M. Spectra of Porphyrins. *J. Mol. Spectrosc.* **1961**, *6*, 138−163.

(18) Gouterman, M. *The Porphyrins*; Elsevier: New York, 1978.

(19) Yum, J.-H.; Jung, I.; Baik, C.; Ko, J.; Nazeeruddin, M. K.; Grätzel, M. High Efficient Donor-Acceptor Ruthenium Complex for Dye-Sensitized Solar Cell Applications. *Energy Environ. Sci.* **2009**, *2*, 100−102.

(20) Zegkinoglou, I.; Ragoussi, M.-E.; Pemmaraju, C. D.; Johnson, P. S.; Pickup, D. F.; Ortega, J. E.; Prendergast, D.; de la Torre, G.; Himpsel, F. J. Spectroscopy of Donor−π−Acceptor Porphyrins for Dye-Sensitized Solar Cells. *J. Phys. Chem. C* **2013**, *117*, 13357−13364.

(21) Scharf, C.; Peter, K.; Bauer, P.; Jung, C.; Thelakkat, M.; Köhler, J. Towards the Characterization of Energy-Transfer Processes in Organic Donor−Acceptor Dyads Based on Triphenyldiamine and Perylenebisimides. *Chem. Phys.* **2006**, *328*, 403−409.

(22) Loudet, A.; Burgess, K. BODIPY Dyes and Their Derivatives: Syntheses and Spectroscopic Properties. *Chem. Rev.* **2007**, *107*, 4891−4932.

(23) Benstead, M.; Mehl, G. H.; Boyle, R. W. 4,4′-Difluoro-4-Bora-3a,4a-Diaza-S-Indacenes (BODIPYs) as Components of Novel Light Active Materials. *Tetrahedron* **2011**, *67*, 3573−3601.

(24) Lazarides, T.; Charalambidis, G.; Vuillamy, A.; Réglier, M.; Klontzas, E.; Froudakis, G.; Kuhri, S.; Guldi, D. M.; Coutsolelos, A. G. Promising Fast Energy Transfer System via an Easy Synthesis: Bodipy−Porphyrin Dyads Connected via a Cyanuric Chloride Bridge, Their Synthesis, and Electrochemical and Photophysical Investigations. *Inorg. Chem.* **2011**, *50*, 8926−8936.

(25) Li, F.; Yang, S. I.; Ciringh, Y.; Seth, J.; Martin, C. H.; Singh, D. L.; Kim, D.; Birge, R. R.; Bocian, D. F.; Holten, D.; Lindsey, J. S. Design, Synthesis, and Photodynamics of Light-Harvesting Arrays Comprised of a Porphyrin and One, Two, or Eight Boron-Dipyrrin Accessory Pigments. *J. Am. Chem. Soc.* **1998**, *120*, 10001−10017.

DOI: 10.1021/acsami.5b00519
ACS Appl. Mater. Interfaces 2015, 7, 8053−8060

(26) Lammi, R. K.; Wagner, R. W.; Ambroise, A.; Diers, J. R.; Bocian, D. F.; Holten, D.; Lindsey, J. S. Mechanisms of Excited-State Energy-Transfer Gating in Linear versus Branched Multiporphyrin Arrays. *J. Phys. Chem. B* **2001**, *105*, 5341−5352.
(27) Gu, Z.-Y.; Guo, D.-S.; Sun, M.; Liu, Y. Effective Enlargement of Fluorescence Resonance Energy Transfer of Poly-Porphyrin Mediated by B-Cyclodextrin Dimers. *J. Org. Chem.* **2010**, *75*, 3600−3607.
(28) Camerel, F.; Ulrich, G.; Barberá, J.; Ziessel, R. Ionic Self-Assembly of Ammonium-Based Amphiphiles and Negatively Charged Bodipy and Porphyrin Luminophores. *Chemistry* **2007**, *13*, 2189−2200.
(29) Lazarides, T.; Kuhri, S.; Charalambidis, G.; Panda, M. K.; Guldi, D. M.; Coutsolelos, A. G. Electron vs Energy Transfer in Arrays Featuring Two Bodipy Chromophores Axially Bound to a Sn(IV) Porphyrin via a Phenolate or Benzoate Bridge. *Inorg. Chem.* **2012**, *51*, 4193−4204.
(30) Leonardi, M. J.; Topka, M. R.; Dinolfo, P. H. Efficient Förster Resonance Energy Transfer in 1,2,3-Triazole Linked BODIPY-Zn(II) Meso-Tetraphenylporphyrin Donor-Acceptor Arrays. *Inorg. Chem.* **2012**, *51*, 13114−13122.
(31) Kursunlu, A. N. Porphyrin−Bodipy Combination: Synthesis, Characterization and Antenna Effect. *RSC Adv.* **2014**, *4*, 47690−47696.
(32) Ganapathi, E.; Madhu, S.; Ravikanth, M. Synthesis and Properties of Triazole Bridged BODIPY-Conjugates. *Tetrahedron* **2014**, *70*, 664−671.
(33) Eggenspiller, A.; Takai, A.; El-Khouly, M. E.; Ohkubo, K.; Gros, C. P.; Bernhard, C.; Goze, C.; Denat, F.; Barbe, J.-M.; Fukuzumi, S. Synthesis and Photodynamics of Fluorescent Blue BODIPY-Porphyrin Tweezers Linked by Triazole Rings. *J. Phys. Chem. A* **2012**, *116*, 3889−3898.
(34) Singh-Rachford, T. N.; Haefele, A.; Ziessel, R.; Castellano, F. N. Boron Dipyrromethene Chromophores: Next Generation Triplet Acceptors/annihilators for Low Power Upconversion Schemes. *J. Am. Chem. Soc.* **2008**, *130*, 16164−16165.
(35) Bohn, P. W. Aspects of Structure and Energy Transport in Artificial Molecular Assemblies. *Annu. Rev. Phys. Chem.* **1993**, *44*, 37−60.
(36) Ozdemir, T.; Atilgan, S.; Kutuk, I.; Yildirim, L. T.; Tulek, A.; Bayindir, M.; Akkaya, E. U. Solid-State Emissive BODIPY Dyes with Bulky Substituents As Spacers. *Org. Lett.* **2009**, *11*, 2105−2107.
(37) Durfor, C. N.; Turner, D. C.; Georger, J. H.; Peek, B. M.; Stenger, D. A. Formation and Naphthoyl Derivatization of Aromatic Aminosilane Self-Assembled Monolayers: Characterization by Atomic Force Microscopy and Ultraviolet Spectroscopy. *Langmuir* **1994**, *10*, 148−152.
(38) Evmenenko, G.; van der Boom, M. E.; Kmetko, J.; Dugan, S. W.; Marks, T. J.; Dutta, P. Specular X-Ray Reflectivity Study of Ordering in Self-Assembled Organic and Hybrid Organic−Inorganic Electro-Optic Multilayer Films. *J. Chem. Phys.* **2001**, *115*, 6722−6727.
(39) Zeppenfeld, A. C.; Fiddler, S. L.; Ham, W. K.; Klopfenstein, B. J.; Page, C. J. Variation of Layer Spacing in Self-Assembled Hafnium-1,10-Decanediylbis(phosphonate) Multilayers As Determined by Ellipsometry and Grazing Angle X-Ray Diffraction. *J. Am. Chem. Soc.* **1994**, *116*, 9158−9165.
(40) Altman, M.; Shukla, A. D.; Zubkov, T.; Evmenenko, G.; Dutta, P.; vanderBoom, M. E. Controlling Structure from the Bottom-Up: Structural and Optical Properties of Layer-by-Layer Assembled Palladium Coordination-Based Multilayers. *J. Am. Chem. Soc.* **2006**, *128*, 7374−7382.
(41) Altman, M.; Zenkina, O.; Evmenenko, G.; Dutta, P.; van der Boom, M. E. Molecular Assembly of a 3D-Ordered Multilayer. *J. Am. Chem. Soc.* **2008**, *130*, 5040−5041.
(42) Chason, E.; Mayer, T. M. Thin Film and Surface Characterization by Specular X-Ray Reflectivity. *Crit. Rev. Solid State Mater. Sci.* **1997**, *22*, 1−67.
(43) Holý, V.; Pietsch, U.; Baumbach, T. *High-Resolution X-Ray Scattering from Thin Films and Multilayers*; Springer Tracts in Modern Physics; Springer: Berlin, 1999; Vol. *149*.
(44) Palomaki, P. K. B.; Krawicz, A.; Dinolfo, P. H. Thickness, Surface Morphology, and Optical Properties of Porphyrin Multilayer Thin Films Assembled on Si(100) Using Copper(I)-Catalyzed Azide-Alkyne Cycloaddition. *Langmuir* **2011**, *27*, 4613−4622.
(45) Tleugabulova, D.; Zhang, Z.; Brennan, J. D. Characterization of Bodipy Dimers Formed in a Molecularly Confined Environment. *J. Phys. Chem. B* **2002**, *106*, 13133−13138.
(46) Tokoro, Y.; Nagai, A.; Chujo, Y. Nanoparticles via H-Aggregation of Amphiphilic BODIPY Dyes. *Tetrahedron Lett.* **2010**, *51*, 3451−3454.
(47) Zhang, D.; Wen, Y.; Xiao, Y.; Yu, G.; Liu, Y.; Qian, X. Bulky 4-Tritylphenylethynyl Substituted Boradiazaindacene: Pure Red Emission, Relatively Large Stokes Shift and Inhibition of Self-Quenching. *Chem. Commun.* **2008**, *39*, 4777−4779.
(48) Fu, Y.-S.; Yu, S. J. Immobilization of Homogeneous Palladium-(II) Complex Catalysts on Novel Polysiloxanes with Controllable Solubility: Important Implications for the Study of Heterogeneous Catalysis on Silica Surfaces This Work Was Supported in Part by the National Science C. *Angew. Chem., Int. Ed.* **2001**, *40*, 437−440.
(49) Song, Y.; Kohlmeir, E. K.; Meade, T. J. Synthesis of Multimeric MR Contrast Agents for Cellular Imaging. *J. Am. Chem. Soc.* **2008**, *130*, 6662−6663.
(50) Chan, T. R.; Hilgraf, R.; Sharpless, K. B.; Fokin, V. V. Polytriazoles as Copper(I)-Stabilizing Ligands in Catalysis. *Org. Lett.* **2004**, *6*, 2853−2855.
(51) Michaels, H. A.; Zhu, L. Ligand-Assisted, Copper(II) Acetate-Accelerated Azide-Alkyne Cycloaddition. *Chem.—Asian J.* **2011**, *6*, 2825−2834.
(52) Wrobel, M.; Aubé, J.; König, B. Parallel Solid-Phase Synthesis of Diaryltriazoles. *Beilstein J. Org. Chem.* **2012**, *8*, 1027−1036.

DOI: 10.1021/acsami.5b00519
ACS Appl. Mater. Interfaces 2015, 7, 8053−8060